Linear Collider Collaboration Tech Notes

Beam Losses in the NLC Extraction Line for High Luminosity Beam Parameters

November 2000

Y. Nosochkov and K. A. Thompson

Stanford Linear Accelerator Center
Stanford, CA

Abstract: In this note we present results of beam tracking in the NLC extraction line for the NLC option with high luminosity beam parameters (Option H). Particle losses for 0.5 TeV and 1 TeV *cms* energy beams have been computed and examined as a function of beam offset at the interaction point (IP). Updated tracking results for the NLC Option A are presented as well.

Beam Losses in the NLC Extraction Line for the High Luminosity Beam Parameters*

Y. Nosochkov and K.A. Thompson
Stanford Linear Accelerator Center, Stanford University, Stanford, CA 94309

Abstract

In this note we present results of beam tracking in the NLC extraction line for the NLC option with high luminosity beam parameters (option H). Particle losses for 0.5 TeV and 1 TeV *cms* energy beams have been computed and examined as a function of beam offset at the interaction point (IP). Updated tracking results for the NLC option A are presented as well.

1 Introduction

Several options for the NLC beam parameters have been under study in the NLC design. The so-called 'baseline' parameter options include options A, B and C for 0.5 TeV and 1 TeV *cms* energy beams [1]–[3]. In addition, a high luminosity option for the beams with nearly-equal β-functions at the IP had been introduced [4]. The beam losses in the NLC extraction line for the 1999 revision of the baseline options had been studied, and the results for option A with 1 TeV *cms* beams can be found in Ref. [5]. The high luminosity option with nearly-equal β-functions had been studied in Ref. [6]. For the current design of the extraction line, the estimated beam loss for the 1999 baseline options is up to 5 kW for 1 TeV *cms* beams and an order of magnitude lower for the 0.5 TeV beams. In the high luminosity case with nearly-equal β-functions the beam loss was unacceptably large mostly due to huge energy spread in the disrupted beam.

Earlier this year (2000), the A, B and C baseline options had been updated and a new high luminosity option (case H) was added [7]. The high luminosity scenario in option H is based on the larger beam current with bunch separation reduced from 2.8 ns to 1.4 ns and on the smaller beam size at IP. In this note we report tracking results for the updated parameter options A and H, and examine effect of the beam offset at IP on the beam loss. The updated parameter options used in this study are shown in Table 1.

2 Tracking Results

The following procedure was used in the tracking study. The beam parameters at the IP listed in Table 1 were used as the input data for the GUINEA-PIG code [8] to generate an incoming gaussian beam distribution and simulate the beam-beam interaction and the disrupted distribution at IP. The resultant distribution was then tracked from IP to the dump and the lost particles were counted and analyzed. Note that only the primary particles were used in this study. The secondary charged particles were not studied and the beamstrahlung photons were assumed to pass to the dump through sufficiently large magnet apertures. Particle tracking was performed using the NLC version of DIMAD code [9]. This modification of DIMAD correctly accounts for energy errors to all orders in the tracking to provide an accurate transmission of the disrupted beams with extremely large energy spread.

*Work supported by Department of Energy contract DE–AC03–76SF00515.

Table 1: NLC beam parameter options [7].

	0.5 TeV				1 TeV			
	A	B	C	H	A	B	C	H
cms Energy [GeV]	510	500	482	490	1022	1000	964	888
Luminosity [10^{33}]	5.3	5.4	5.5	22	10.6	10.8	11	34
Repetition rate [Hz]	120	120	120	120	120	120	120	120
Bunch charge [10^{10}]	0.7	0.82	1	0.75	0.7	0.82	1	0.75
Bunches/RF-pulse	95	95	95	190	95	95	95	190
Bunch separation [ns]	2.8	2.8	2.8	1.4	2.8	2.8	2.8	1.4
Eff. gradient [MV/m]	58.7	57.3	55.2	50.2	58.7	57.3	55.2	50.2
Inj. $\gamma\epsilon_x/\gamma\epsilon_y$ [10^{-8} m]	300/3	300/3	300/3	300/2	300/3	300/3	300/3	300/2
$\gamma\epsilon_x$ at IP [10^{-8} m]	400	450	500	360	400	450	500	360
$\gamma\epsilon_y$ at IP [10^{-8} m]	6.5	8.5	12	3.5	6.5	8.5	12	3.5
β_x/β_y at IP [mm]	12/0.12	12/0.12	13/0.15	8/0.1	12/0.12	12/0.12	13/0.15	10/0.12
σ_x/σ_y at IP [nm]	310/4	330/4.6	365/6.2	245/2.7	219/2.8	235/3.2	260/4.4	204/2.2
σ_z at IP [μm]	90	120	140	110	90	120	140	110
Υ_{ave}	0.11	0.09	0.08	0.11	0.32	0.25	0.23	0.26
Pinch enhancement	1.46	1.35	1.39	1.43	1.46	1.35	1.39	1.49
Beamstrahlung δB [%]	3.2	3	3	4.6	8.3	8.1	8.4	8.8
Photons per e^+/e^-	0.86	0.96	1.05	1.17	1.12	1.25	1.38	1.33
Two linac length [km]	5	5	5	5.4	9.9	9.9	9.9	9.9

The extraction line optics is shown in Fig. 1 where the beam travels from the left (IP) to the right (dump) [6]. The optics consists of the following modules. The six quadrupole system after IP is designed to minimize energy dependent deflections in the quadrupoles and focus the beam to the secondary IP which is located in the middle of the downstream chicane. The chicane consists of four vertical double bends to generate 2 cm vertical dispersion at the secondary IP for energy spectrum measurements and measurements with Compton polarimeter [10]. The last four quadrupoles generate a wide parallel beam at the dump.

In the tracking we assumed that there are no machine errors in the extraction line. The vertical orbit generated in the 6 T detector solenoid was compensated by the proper vertical alignment of the downstream magnets.

2.1 Disrupted Beam Parameters at IP

Tables 2–5 list the IP parameters of the disrupted distributions for 0.5 TeV and 1 TeV *cms* energy beams with $5{\cdot}10^4$ generated particles in options A and H. The notations used in Tables 2–5 refer to the horizontal X, X', vertical Y, Y' and longitudinal Z coordinates and energy error $\frac{\Delta E}{E}$. The listed parameters are for zero beam offset at the IP and monochromatic incoming beam (no initial energy spread). The realistic incoming energy spread is about $\pm 0.5\%$, but it is negligible compared to huge energy spread generated in the collision and should not affect the results of this study. Dependence on the beam offset will be discussed later in this report. Since the incoming gaussian beam is centered at zero in all six phase space coordinates, the disrupted IP distribution is also centered at zero except $\frac{\Delta E}{E}$ which is shifted towards lower energies.

For the NLC beam parameters, the beam-beam interaction significantly distorts the beam distribution. Comparison of the beam parameters just before and after collision (Tables 1 and 2–5,

Table 2: Disrupted IP parameters in option A with E_{cms} =510 GeV.

	X [nm]	X' [μrad]	Y [nm]	Y' [μrad]	Z [μm]	$\frac{\Delta E}{E}$ [%]
rms	309	144	4.4	50	89	6.6
maximum	1468	382	35.1	279	284	-64.2
average	0.4	-0.2	0.0	0.2	0.0	-3.1

Table 3: Disrupted IP parameters in option H with E_{cms} =490 GeV.

	X [nm]	X' [μrad]	Y [nm]	Y' [μrad]	Z [μm]	$\frac{\Delta E}{E}$ [%]
rms	245	211	4.6	39	109	8.1
maximum	1085	633	28.3	233	348	-66.7
average	0.3	-0.4	0.0	0.0	0.3	-4.6

Table 4: Disrupted IP parameters in option A with E_{cms} =1022 GeV.

	X [nm]	X' [μrad]	Y [nm]	Y' [μrad]	Z [μm]	$\frac{\Delta E}{E}$ [%]
rms	220	108	3.1	35	88	12.5
maximum	1053	677	27.3	216	285	-87.2
average	-1	0.5	0.0	0.0	-0.3	-7.4

Table 5: Disrupted IP parameters in option H with E_{cms} =888 GeV.

	X [nm]	X' [μrad]	Y [nm]	Y' [μrad]	Z [μm]	$\frac{\Delta E}{E}$ [%]
rms	204	143	3.4	28	109	12.4
maximum	841	693	21.8	173	348	-83.0
average	0.0	0.0	0.0	0.2	-0.6	-8.0

respectively) shows that the beam angular divergence increases up to several times and very large low energy tail is generated. The disrupted beam emittance and lattice functions at the IP can be deduced from the beam distribution as well. Table 6 compares the beam phase space parameters and lattice functions before and after collision for the A and H cases. Note a higher beam emittance for the disrupted beam mostly due to increased beam divergence.

An example of disrupted IP distribution in the X, X', Y, Y' directions is shown in Fig. 2–5 for option H with *cms* energy of 490 GeV. Note that the X'-distribution has a double-peak shape which is characteristic for the flat beam collisions. Since the extraction line has a point-to-parallel transformation from the IP to the dump, this X'-distribution is translated into a double-peak X-distribution at the dump.

Table 6: IP parameters before and after beam-beam collision.

Option	A		H		A		H	
cms Energy [GeV]	510		490		1022		888	
Collision	before	after	before	after	before	after	before	after
$\gamma\epsilon_x$ [10^{-8} m]	400	1046	360	1175	400	1152	360	1215
$\gamma\epsilon_y$ [10^{-8} m]	6.5	10.6	3.5	7.2	6.5	10.8	3.5	6.8
β_x [mm]	12	4.55	8	2.44	12	4.18	10	2.96
β_y [mm]	0.12	0.09	0.1	0.14	0.12	0.09	0.12	0.15
α_x	0	1.870	0	1.852	0	1.787	0	1.828
α_y	0	0.207	0	0.675	0	0.231	0	0.656
X_{rms} [nm]	310	309	245	245	219	220	204	204
Y_{rms} [nm]	4.0	4.4	2.7	4.6	2.8	3.1	2.2	3.4
X'_{rms} [μrad]	26	144	31	211	18	108	20	143
Y'_{rms} [μrad]	33	50	27	39	23	35	18	28

2.2 Particle Loss in the Extraction Line

The $5{\cdot}10^4$ particle disrupted distributions described above were tracked from the IP to the dump and the data for lost particles were collected. In agreement with our previous studies [5, 6], this tracking confirmed that particle losses occur only in the very low energy tail. In fact, no particles were lost in options A and H with 0.5 TeV *cms* energy beams because the low energy tail at this energy is not as large as at 1 TeV. However, one should keep in mind that only primary particles were considered in this study, and there may be particle losses if higher statistics is used and optics and beam errors are applied, however these losses are expected to be reasonably low.

Fig. 6–9 show the IP energy distribution for the survived (thin histogram) and lost (thick) particles in the extraction line for options A and H with 0.5 TeV and 1 TeV *cms* beams. One can see that for the NLC beam parameters the low energy bandpass in the extraction line is close to $\frac{\Delta E}{E} = -70\%$.

Based on the number of lost particles and their energy, the beam power loss P_{loss} can be calculated using the following formula:

$$P_{loss}[W] = 1.602{\cdot}10^{-10}\,\frac{N_b n_b E[GeV] f[s^{-1}]}{N_{track}} \sum_{i=1}^{N_{loss}} (1 + \frac{\Delta E_i}{E}), \qquad (1)$$

where N_b is the number of particles per bunch, n_b the number of bunches per RF-pulse, E the nominal beam energy, f the repetition rate, N_{track} the total number of particles in tracking, and N_{loss} the number of lost particles in tracking. Total beam losses for options A and H are listed in Table 7. Note that in case H with 1 TeV *cms* beams the relative number of lost particles is less than in case A, but the beam power loss is greater due to the higher number of bunches per RF-pulse.

The distribution of particle losses along the beam-line was further analyzed for the 1 TeV beams. Fig. 10, 11 show power loss per meter $\frac{dP_{loss}}{ds}$ in options A and H. Due to rather low statistics of the lost particles in the tracking the amplitude of $\frac{dP_{loss}}{ds}$ in Fig. 10, 11 may not be very accurate. The realistic values of $\frac{dP_{loss}}{ds}$ are likely to be lower. Also, the relatively higher peaks of $\frac{dP_{loss}}{ds}$ in Fig. 10 compared to Fig. 11 are caused by a few particles lost in very short length drifts in option A.

Table 7: Beam loss in tracking with $5 \cdot 10^4$ particles.

Option	A	H	A	H
cms Energy [GeV]	510	490	1022	888
Lost particles [%]	0	0	0.088	0.054
Power loss [kW]	0	0	1.34	1.66

Fig. 12, 13 show the positions in the extraction line where the particles were lost (each circle corresponds to a particle) and their energy error $\frac{\Delta E}{E}$. Naturally, particles with the lowest energy are lost first since the energy dependent deflections in the quadrupoles increase hyperbolically as $\frac{1}{E}$. One can conclude from Fig. 12, 13 that particles with $\frac{\Delta E}{E}$ below -75% almost certainly will be lost in the first six quadrupoles after IP. Note that the realistic energy bandpass may be smaller if machine and beam errors are included.

Azimuth positions of the particles at the locations where they were lost are shown in Fig. 14, 15. In these Figures, the azimuth angle is $\theta = \arctan \frac{y}{x}$, where $\theta = 0, \pm 180^\circ$ corresponds to the horizontal plane and $\theta = \pm 90^\circ$ to the vertical plane. Fig. 14, 15 indicate that under nominal conditions the particles are more likely to be lost in the horizontal plane, possibly due to larger horizontal beam size. Note that at such low energies the corresponding β-functions and beam size are significantly perturbed compared to the nominal energy functions. The lowest energy particles may be lost at any angle in the six quadrupole system after IP due to the fast increase in their deflections.

Finally, an example of horizontal and vertical particle distribution at the dump for option H with $E_{cms} = 490$ GeV is shown in Fig. 16, 17. The double peak X-distribution is the result of the double peak X'-distribution at the IP and point-to-parallel transformation from IP to the dump.

2.3 Particle Loss vs. Beam Offset at IP

The beam loss in the extraction line depends on parameters of the disrupted particle distribution at the IP. Various incoming beam errors may affect the beam-beam interaction and alter the disrupted distribution. In this study, we investigated the effect of beam-to-beam horizontal and vertical offset at the IP on beam losses in the extraction line for option H with $E_{cms} = 490$ GeV.

In GUINEA-PIG simulations the two colliding beams were symmetrically and oppositely displaced at the IP by half of the total beam offset $\pm\frac{1}{2}\Delta x$ or $\pm\frac{1}{2}\Delta y$, and the disrupted IP distributions were generated for various values of Δx and Δy. These distributions with $5 \cdot 10^4$ particles were tracked in the extraction line for analysis of the particle losses as a function of beam offset at IP.

At the two extreme values of the beam offset, $\Delta x = \Delta y = \infty$ and $\Delta x = \Delta y = 0$, the IP disrupted parameters are already given in Tables 1 and Tables 2–5, respectively. Obviously, as the beam offset increases the disrupted distribution should eventually converge to the incoming beam distribution since less interaction takes place. Note, however, that even though the very large offset may not disrupt the beam distribution, it still may result in beam loss due to large incoming beam orbit.

Summary of disrupted IP beam parameters as a function of beam offset at IP for option H with $E_{cms} = 490$ GeV is given in Table 8 where the notations *ave* and *max* refer to average and maximum values respectively and $\sigma_{x,y}$ is the undisrupted *rms* beam size at IP. One can see that the x-offset gradually reduces the effect of beam-beam interaction, and the disrupted parameters monotonically converge to the undisrupted values at large Δx. On the contrary, the y-offset initially increases the disruptive effect on the energy spread and the vertical beam size. The *rms* and average values of

Table 8: Disrupted IP parameters vs. beam offset at IP in option H with $E_{cms}=490$ GeV.

Offset		X_{rms} [nm]	X'_{rms} [μrad]	Y_{rms} [nm]	Y'_{rms} [μrad]	$(\frac{\Delta E}{E})_{ave}$ [%]	$(\frac{\Delta E}{E})_{rms}$ [%]	$(\frac{\Delta E}{E})_{max}$ [%]	Z_{rms} [μm]
0		244.7	210.8	4.63	39.4	-4.62	8.13	-66.7	108.6
$\Delta x=$	$1\sigma_x$	244.9	157.7	4.35	36.9	-4.25	7.71	-66.4	108.1
	$2\sigma_x$	246.5	90.4	3.60	32.0	-3.13	6.39	-72.5	108.6
	$4\sigma_x$	243.0	62.7	2.75	27.4	-0.78	2.66	-40.2	109.1
$\Delta y=$	$1\sigma_y$	245.9	206.8	8.22	64.6	-4.98	8.43	-79.2	108.9
	$2\sigma_y$	244.5	202.2	10.46	82.4	-5.41	8.91	-75.5	108.9
	$4\sigma_y$	245.7	192.4	11.91	88.9	-5.57	9.06	-72.7	108.3
	$10\sigma_y$	246.5	202.3	14.91	95.6	-6.46	9.89	-71.6	109.0
	$15\sigma_y$	244.6	196.0	16.23	109.1	-6.79	10.13	-76.0	108.7
	$20\sigma_y$	244.7	187.1	17.27	113.8	-6.69	10.05	-69.9	108.5
	$30\sigma_y$	245.1	167.8	17.27	109.5	-6.11	9.50	-70.8	108.8
	$40\sigma_y$	244.9	48.4	4.94	60.3	-0.59	2.49	-46.0	108.3

the energy spread maximize at about $\Delta y \approx 15\sigma_y$, and the beam vertical size and divergence reach maximum at $\Delta y \approx 20\sigma_y$. Fig. 18–21 show that these maximums are rather broad and, relatively, the vertical beam size and divergence are blown up the most. In the horizontal plane, the beam size and divergence are not adversely affected by the beam offset. The values of $(\frac{\Delta E}{E})_{max}$ in Table 8 may not be very accurate due to limited statistics.

A comparison of the disrupted energy spread at the vertical beam offset of $\Delta y = 0$, $15\sigma_y$ and $40\sigma_y$ is shown in Fig. 22. The effect of the beam blow up is shown in more detail in Table 9 where the disrupted IP parameters for beam offsets of $\Delta y = 0$ and $20\sigma_y$ are compared. Note that the vertical emittance is blown up more than ten times at $\Delta y = 20\sigma_y$.

As a result of the increased energy spread and vertical beam size, one can also expect higher beam loss in the extraction line for IP offset values near Δy = 15–$20\sigma_y$. Beam tracking was

Table 9: Disrupted IP parameters for beam offsets of $\Delta y = 0$ and $20\sigma_y$ in option H with E_{cms} = 490 GeV.

Δy	0	$20\sigma_y$
$\gamma\epsilon_x$ [10^{-8} m]	1175	1068
$\gamma\epsilon_y$ [10^{-8} m]	7.2	94.2
β_x [mm]	2.44	2.69
β_y [mm]	0.14	0.15
α_x	1.852	1.796
α_y	0.675	-0.0002
X_{rms} [nm]	245	245
Y_{rms} [nm]	4.6	17.3
X'_{rms} [μrad]	211	187
Y'_{rms} [μrad]	39	114

performed for all of the above offsets and the results are shown in Fig. 23 where the number of lost particles is plotted against the beam y-offset at IP. The maximum beam loss occurs at $\Delta y = 20\sigma_y$ and amounts to 0.69 kW of power loss with 15 lost particles out of $5 \cdot 10^4$ in tracking. Some irregularities in Fig. 23 are due to low statistics of the lost particles.

Tracking results with non-zero horizontal IP offsets showed no beam loss in option H with $E_{cms} = 490$ GeV. That is because the x-offset actually reduces the disruption of the beam emittance and energy spread as shown in Table 8.

To identify the sources of beam loss with a non-zero vertical IP offset we analyzed particle loss distribution for the case with the maximum beam loss at $\Delta y = 20\sigma_y$. Energy distribution at IP for the survived and lost particles in this case is shown in Fig. 24. Fig. 25 shows power loss per meter in the extraction line, though with only 15 lost particles the accuracy of $\frac{dP_{loss}}{ds}$ may not be very good. Fig. 26 shows the azimuth positions of the lost particles. All of the particles except one were lost in the vertical plane near $\theta = \pm 90°$. That means that the blow up of the vertical emittance is the main reason for the higher particle loss with a non-zero vertical beam offset.

Our expectation is that the power loss due to beam IP offset, even at the maximum level of 0.69 kW, can be safely disposed. In practice, these losses should be much lower since the beam offset will be controlled to keep the luminosity at maximum. We expect that actual vertical beam offsets will be on the order of $1\sigma_y$ which corresponds to about 15 times less power loss compared to the maximum in Fig. 23. To estimate more accurately the beam loss with $\Delta y = 1\sigma_y$, we tracked $2 \cdot 10^5$ particles in the extraction line. This resulted in 4 lost particles with the total power loss of 0.036 kW in option H with $E_{cms} = 490$ GeV.

3 Summary

In this study, we computed beam losses in the extraction line for options A and H of the NLC beam parameters. Under ideal conditions in the beam-line and without beam errors there were no particle losses in tracking with 0.5 TeV *cms* energy beams. With 1 TeV *cms* beams the computed power loss amounted to 1.34 kW in option A and 1.66 kW in option H. We expect that this level of beam loss can be safely handled in the extraction line. Compared to the last year (1999) version of option A, the power loss is reduced a factor of three for the updated options A and H.

For option H with $E_{cms} = 490$ GeV, we investigated the effect of beam IP offset on the beam loss. The horizontal offsets do not have adverse affects on the beam loss since the beam disruption is actually reduced. The vertical offsets initially increase the beam disruption and result in the maximum power loss of 0.69 kW at $\Delta y = 20\sigma_y$. At more realistic offset of $\Delta y = 1\sigma_y$ the computed power loss was 0.036 kW.

We expect similar increase in the beam loss as a function of IP y-offset for 1 TeV *cms* beams. This study will have to be done in the future. We also need to evaluate the effects of other beam and machine errors.

References

[1] T. Raubenheimer, K. Yokoya, "*Parameters for the JLC/NLC*," SLAC note LCC–0003 (1998).

[2] T. Raubenheimer, K. Thompson, "*High Luminosity Options at 500 GeV cms*," SLAC note LCC–0004 (1998).

[3] T.O. Raubenheimer, K.A. Thompson, "*Luminosity for NLC Design Variations*," SLAC note LCC–0014 (1999).

[4] K.A. Thompson, T.O. Raubenheimer, P. Tenenbaum, "*High-luminosity NLC Designs with Near-equal Horizontal and Vertical Beta Functions*," SLAC note LCC–0022 (1999).

[5] Y. Nosochkov, *et al.*, "*The Next Linear Collider Extraction Line Design*," SLAC–PUB–8096 (1999).

[6] Y.M. Nosochkov and T.O. Raubenheimer, "*NLC Extraction Line Studies*," SLAC–PUB–8313 and LCC–0034 (1999).

[7] http://www-project.slac.stanford.edu/lc/local/AccelPhysics/Accel_Physics_index.htm.

[8] D. Schulte, TESLA–97–08 (1996).

[9] P. Tenenbaum, *et al.*, "*Use of Simulation Programs for the Modeling of the Next Linear Collider*," SLAC–PUB–8136 (1999).

[10] Y. Nosochkov and T.O. Raubenheimer, "*Study of Beam Energy Spectrum Measurement in the NLC Extraction Line*," SLAC note LCC–0045 (2000).

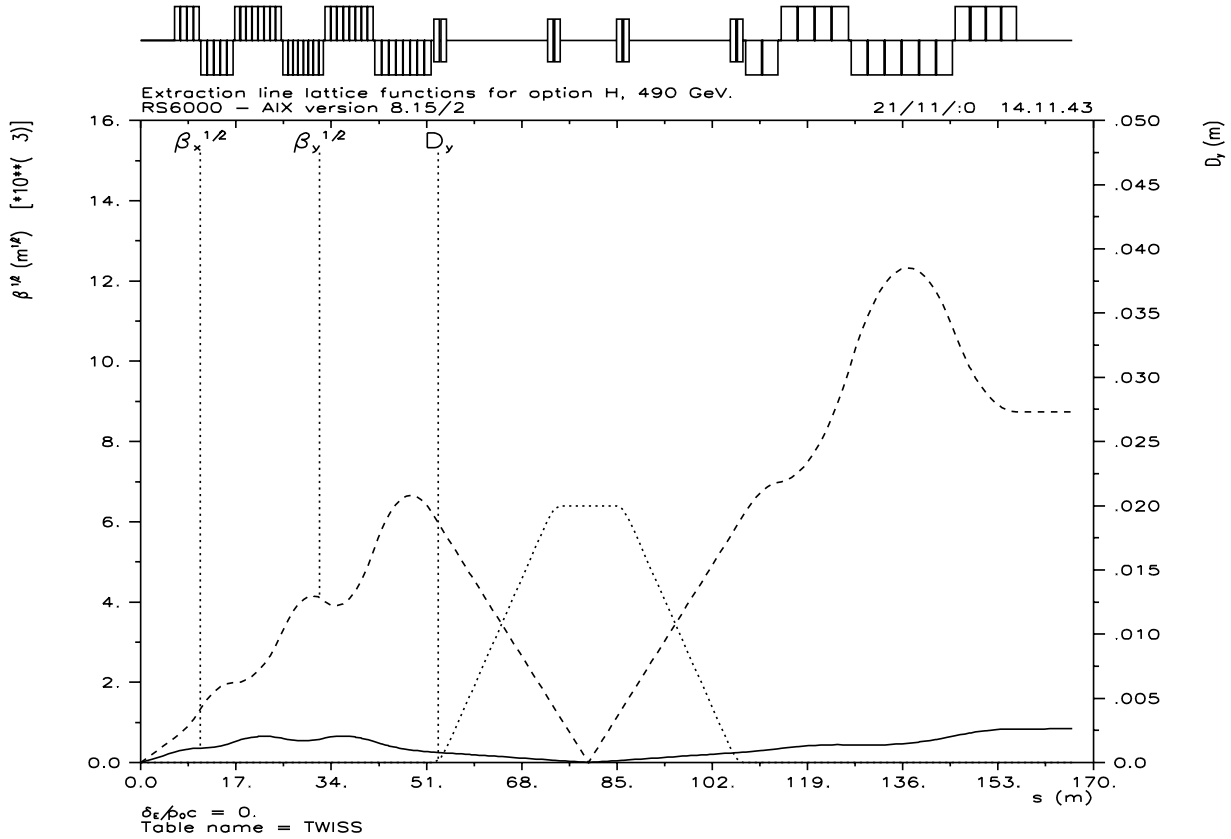

Figure 1: NLC extraction line with disrupted lattice functions ($\sqrt{\beta_{x,y}}$ and η_y) for option H with E_{cms} =490 GeV (IP is on the left).

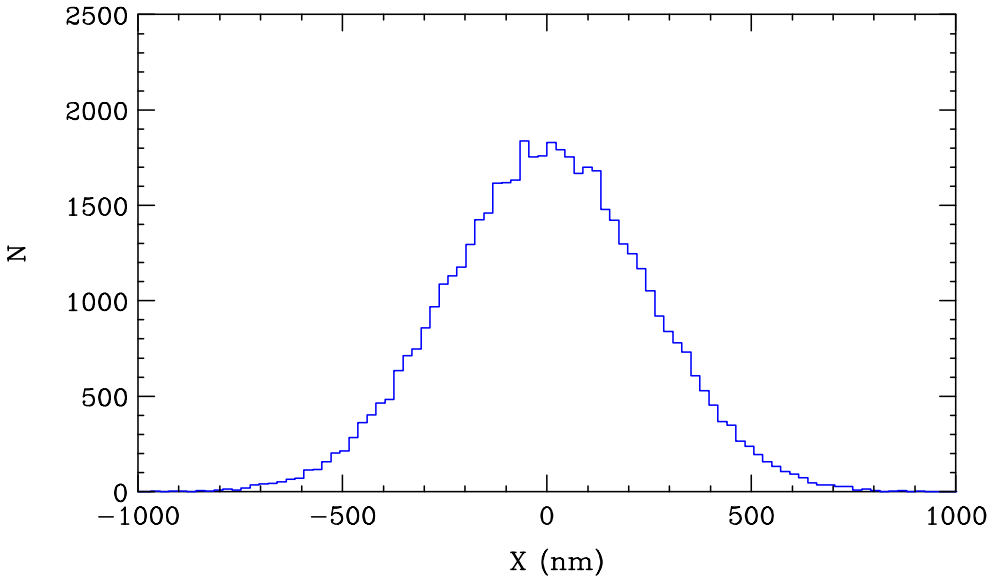

Figure 2: Disrupted X-distribution at IP in option H with $E_{cms} = 490$ GeV.

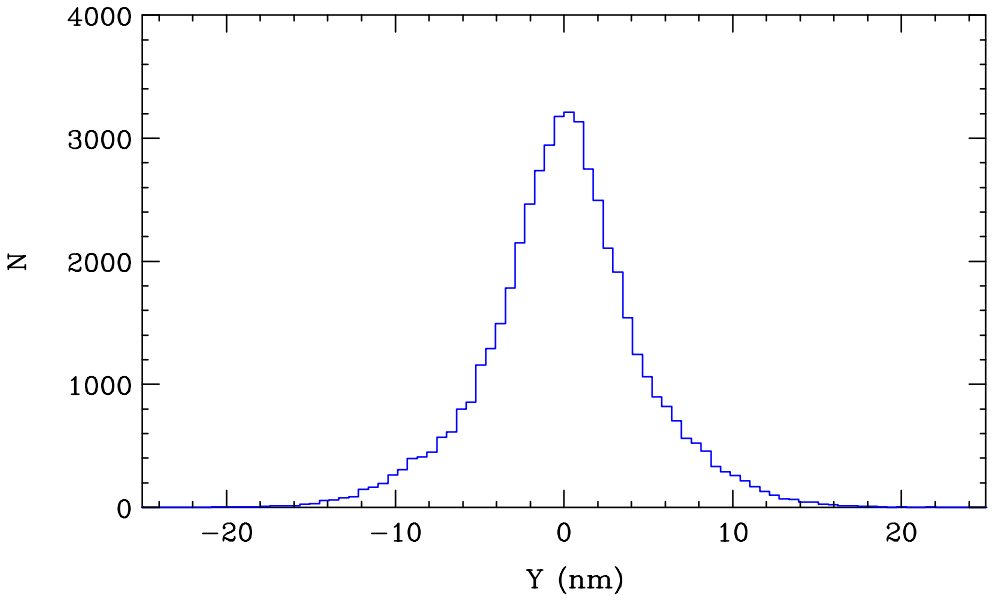

Figure 3: Disrupted Y-distribution at IP in option H with $E_{cms} = 490$ GeV.

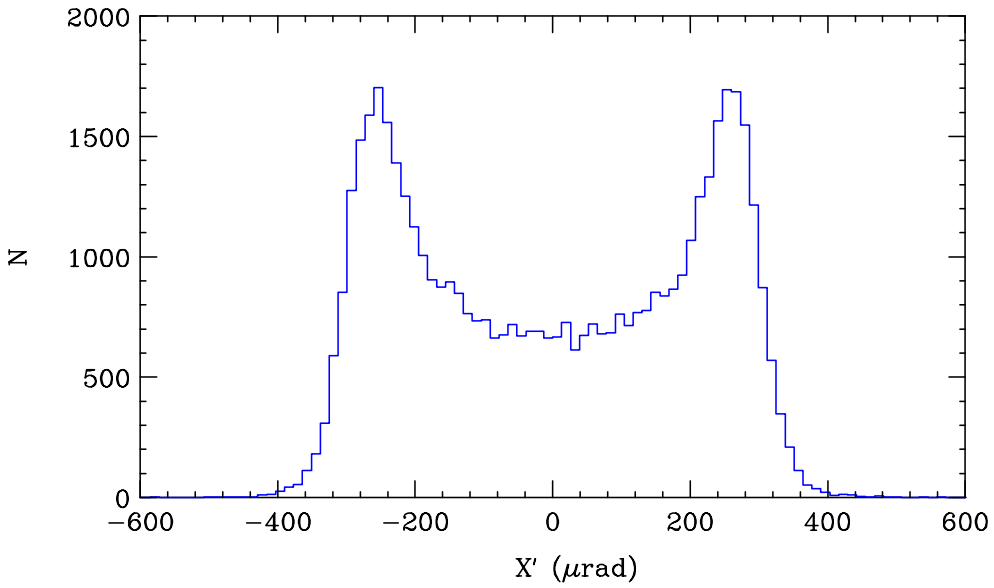

Figure 4: Disrupted X'-distribution at IP in option H with $E_{cms} = 490$ GeV.

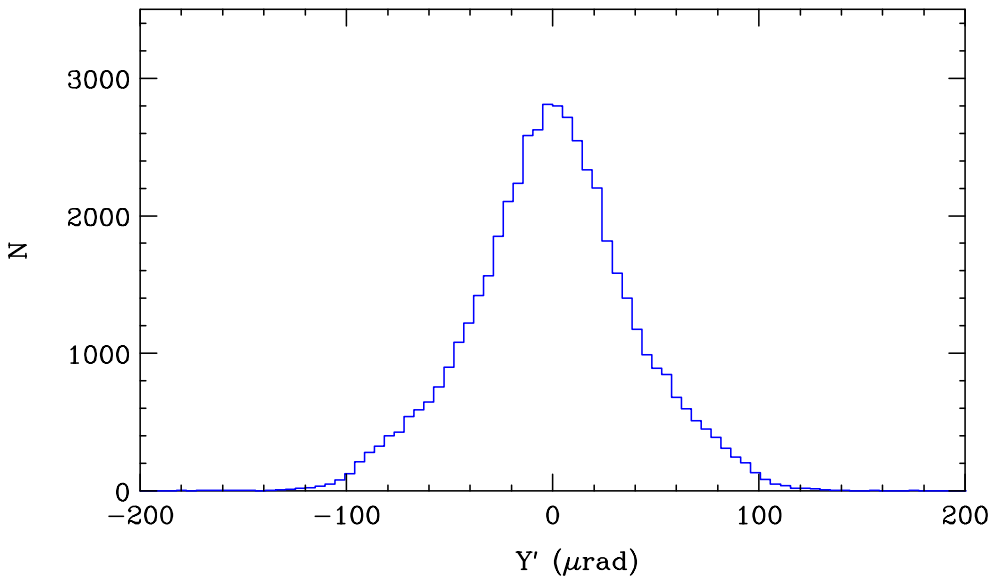

Figure 5: Disrupted Y'-distribution at IP in option H with $E_{cms} = 490$ GeV.

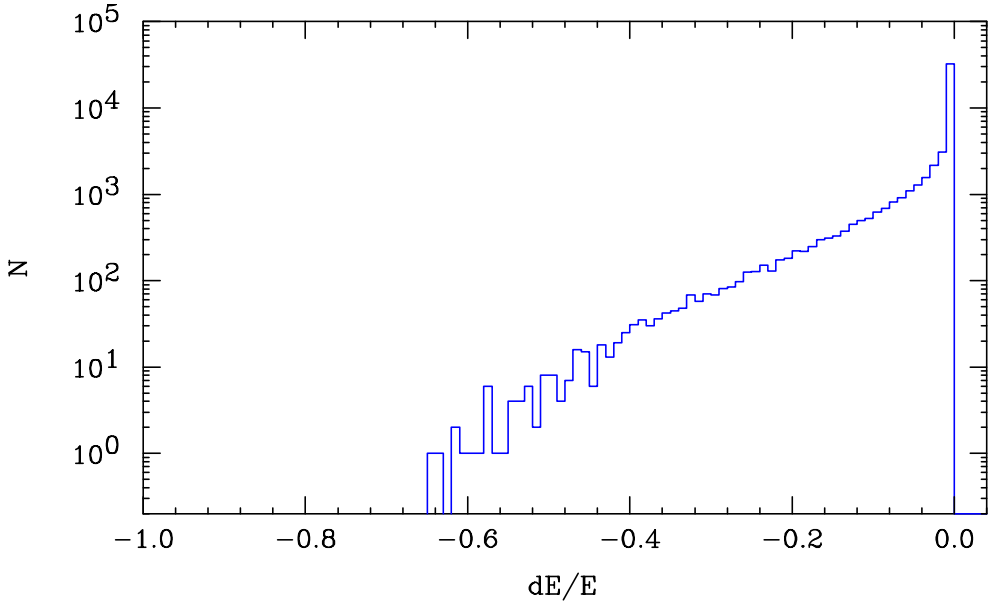

Figure 6: Disrupted energy distribution at IP in option A with E_{cms} =510 GeV.

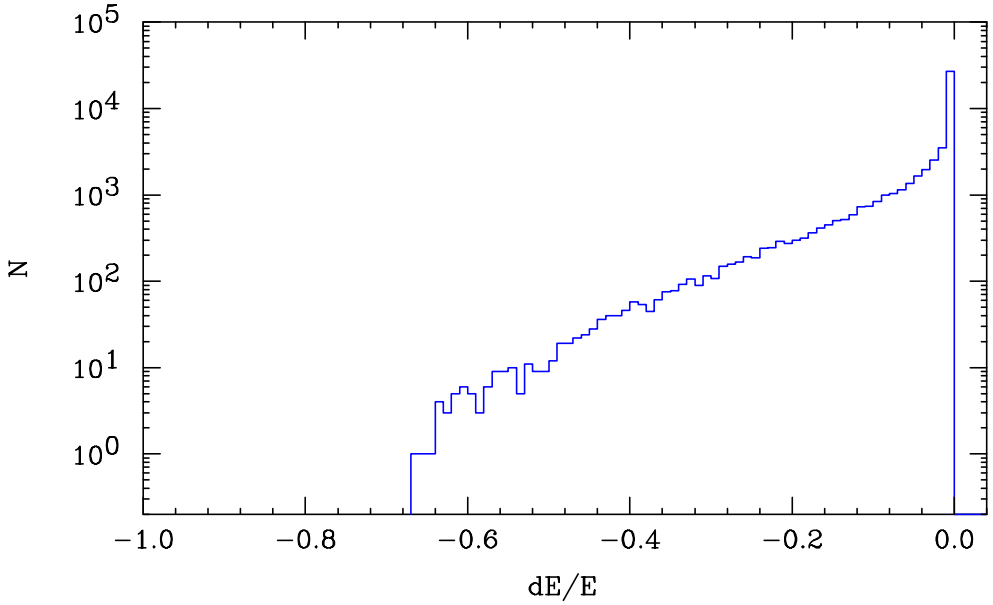

Figure 7: Disrupted energy distribution at IP in option H with E_{cms} =490 GeV.

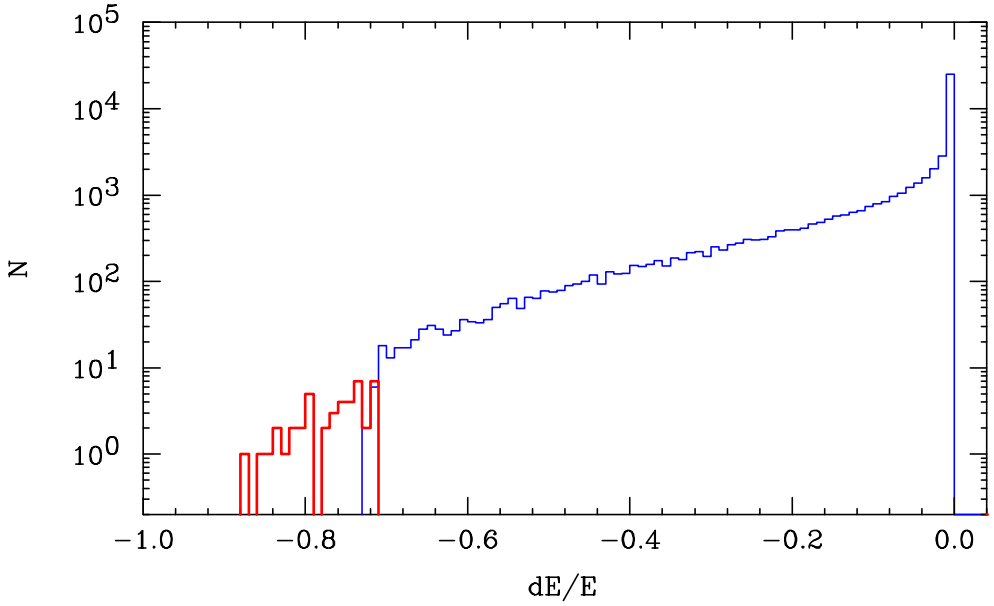

Figure 8: Disrupted energy distribution at IP for survived (thin line) and lost (thick) particles in option A with $E_{cms} = 1022$ GeV.

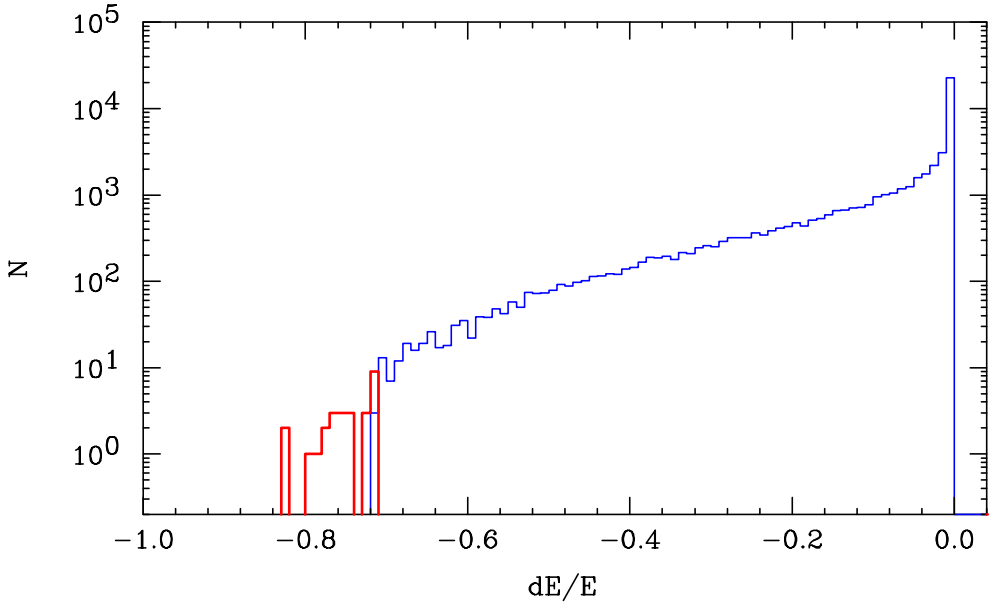

Figure 9: Disrupted energy distribution at IP for survived (thin line) and lost (thick) particles in option H with $E_{cms} = 888$ GeV.

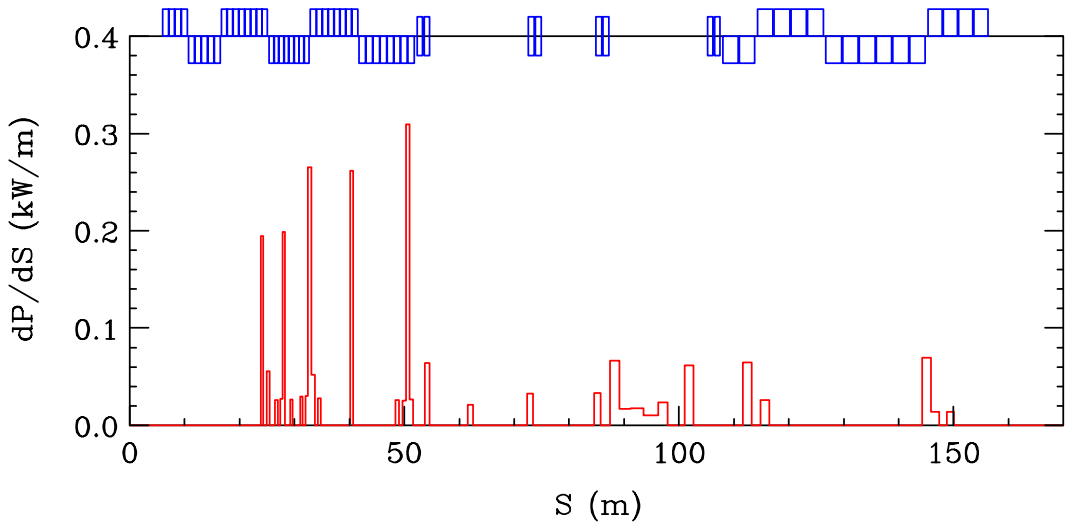

Figure 10: Beam power loss per meter $\frac{dP_{loss}}{ds}$ in the extraction line in option A with $E_{cms} = 1022$ GeV.

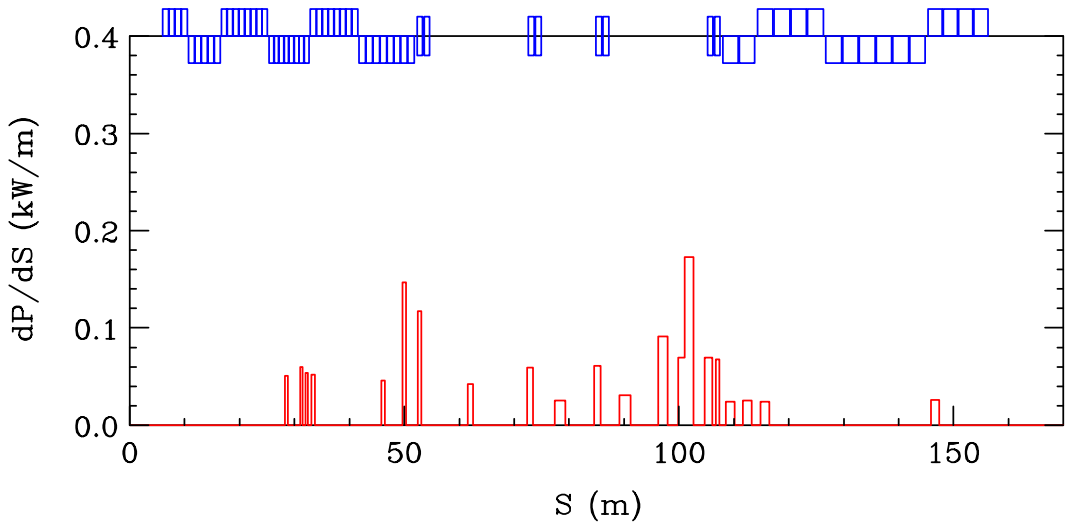

Figure 11: Beam power loss per meter $\frac{dP_{loss}}{ds}$ in the extraction line in option H with $E_{cms} = 888$ GeV.

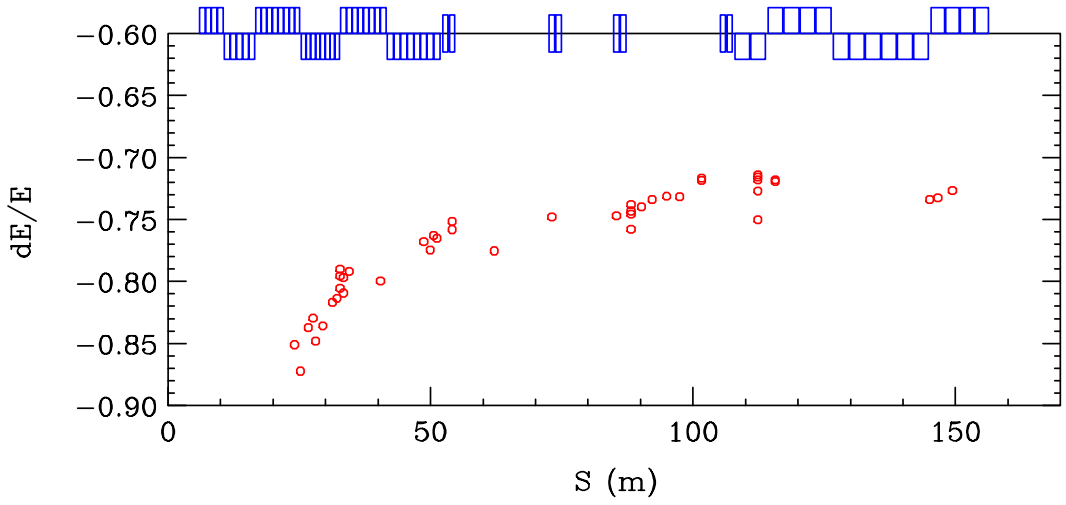

Figure 12: Longitudinal positions of lost particles and their energy error in option A with $E_{cms} =$ 1022 GeV.

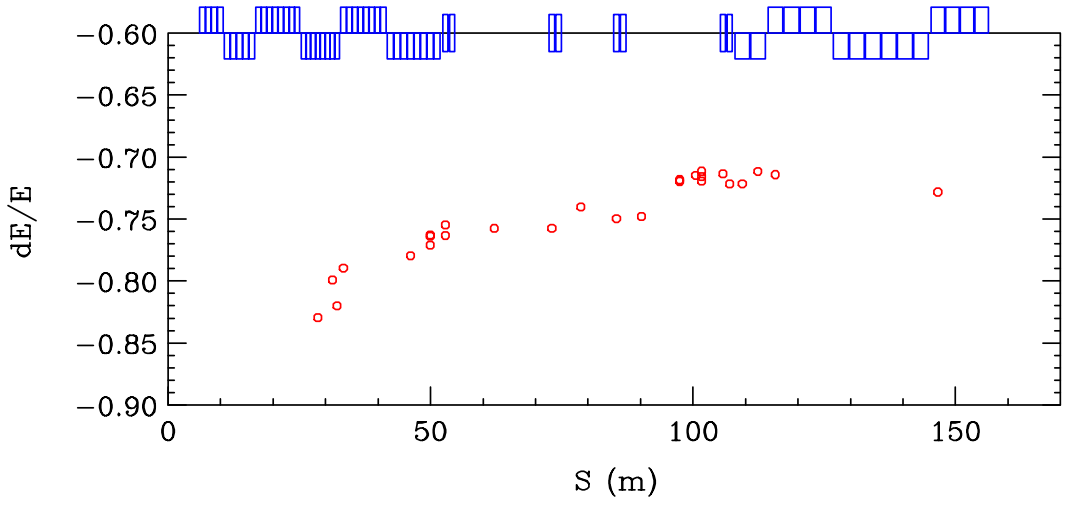

Figure 13: Longitudinal positions of lost particles and their energy error in option H with $E_{cms} =$ 888 GeV.

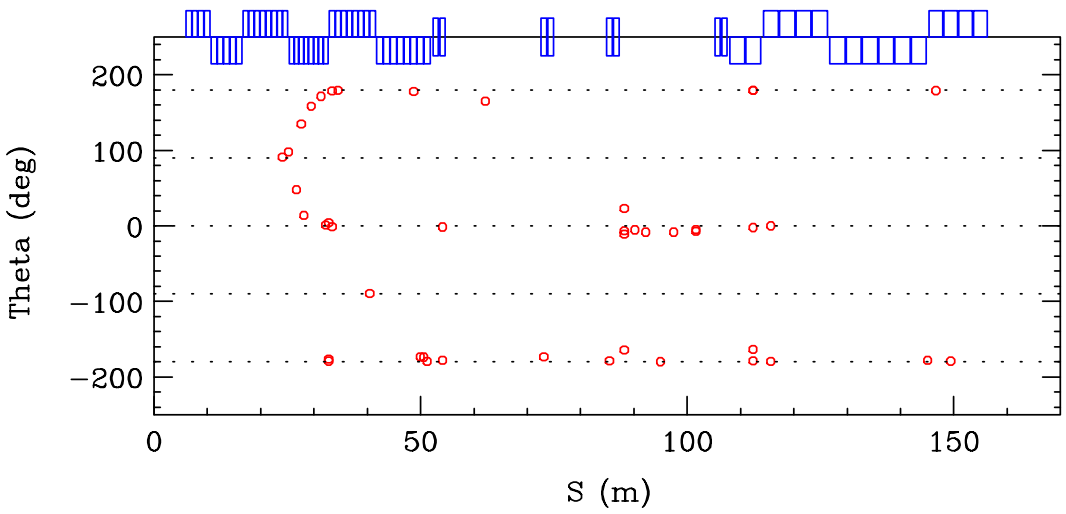

Figure 14: Azimuth positions of lost particles in the extraction line in option A with E_{cms} = 1022 GeV.

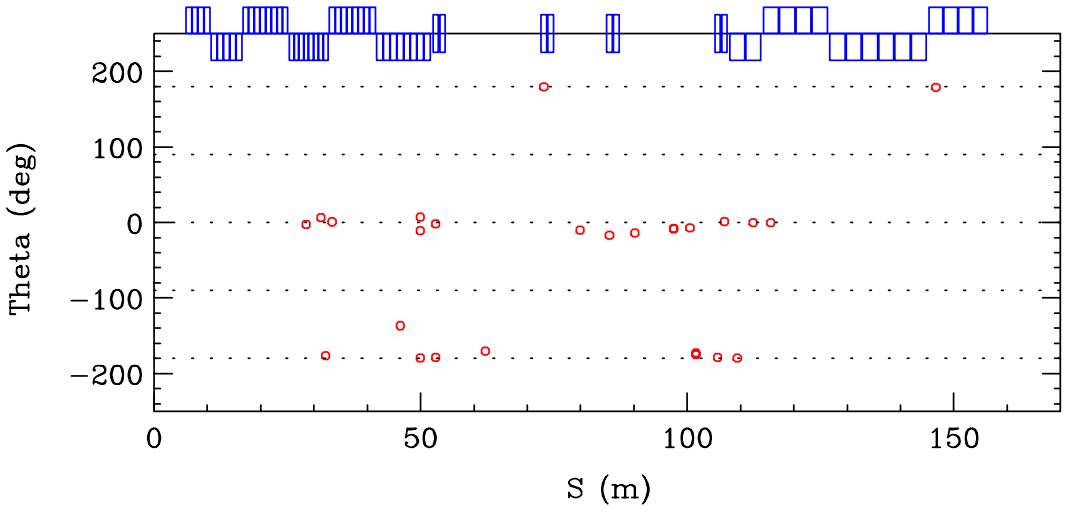

Figure 15: Azimuth positions of lost particles in the extraction line in option H with E_{cms} = 888 GeV.

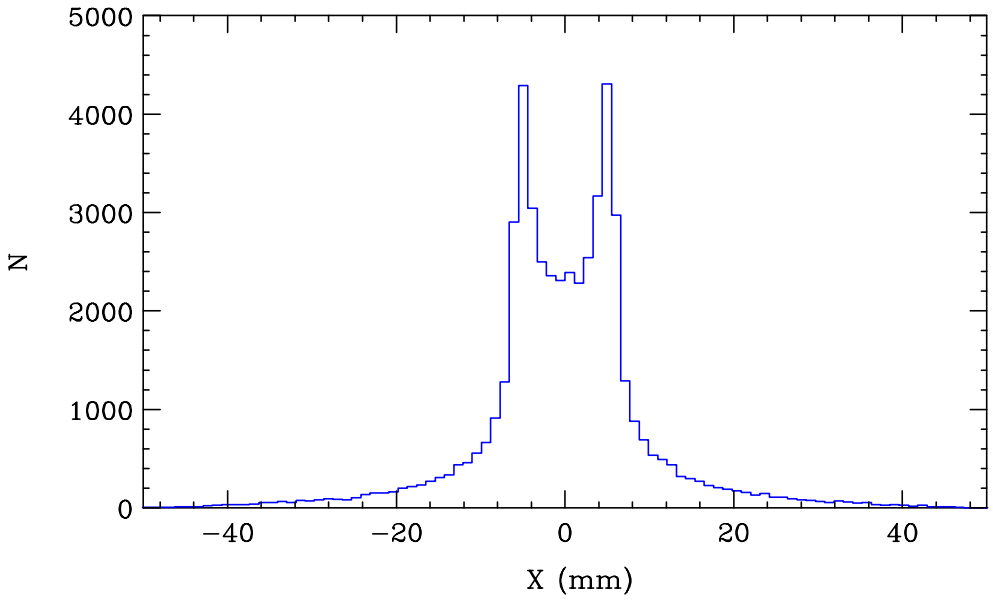

Figure 16: Horizontal distribution at the dump in option H with $E_{cms} = 490$ GeV.

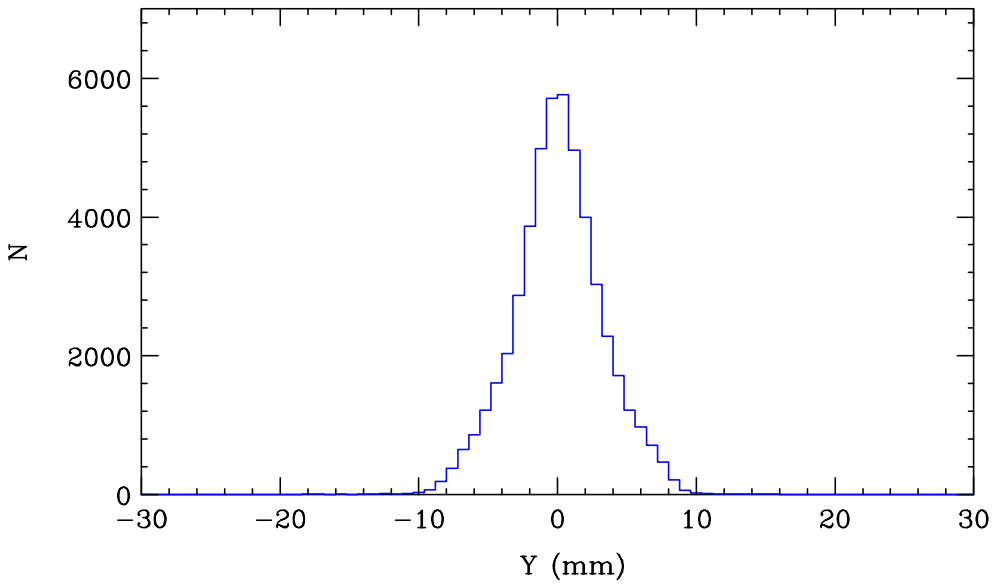

Figure 17: Vertical distribution at the dump in option H with $E_{cms} = 490$ GeV.

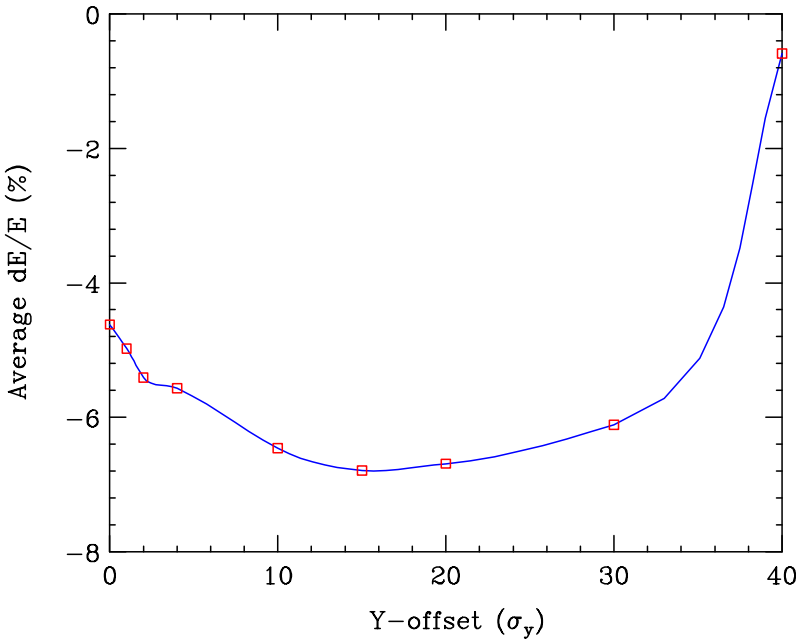

Figure 18: Disrupted average $\frac{\Delta E}{E}$ at IP vs. beam IP offset Δy (in undisrupted σ_y) in option H with $E_{cms} = 490$ GeV.

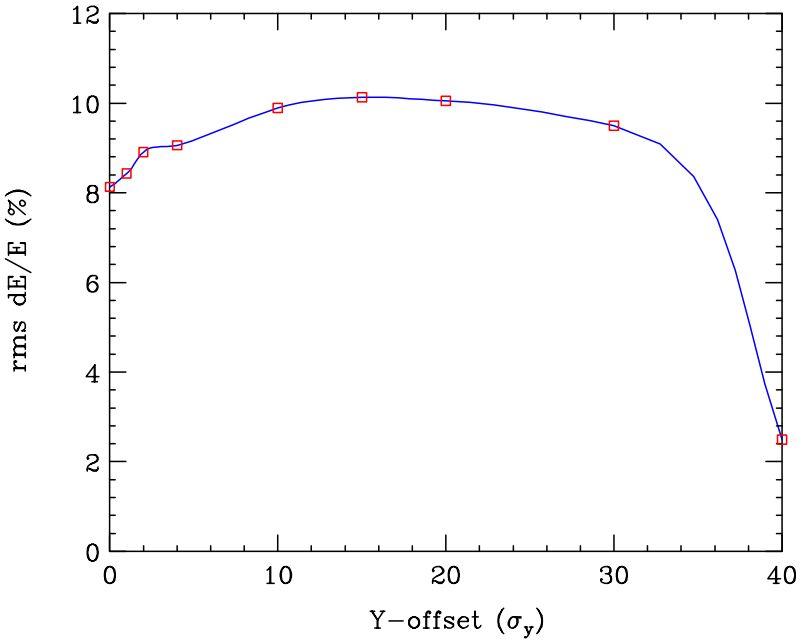

Figure 19: Disrupted rms $\frac{\Delta E}{E}$ at IP vs. beam IP offset Δy (in undisrupted σ_y) in option H with $E_{cms} = 490$ GeV.

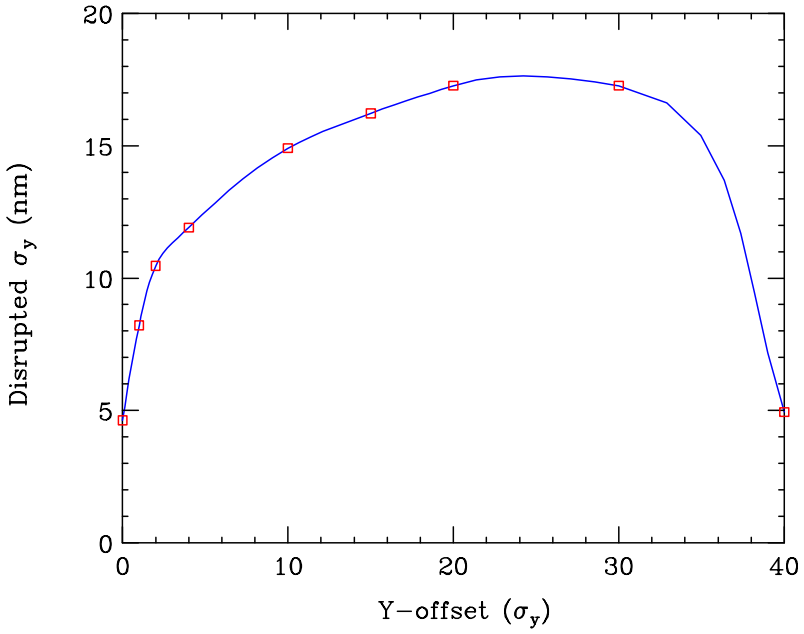

Figure 20: Disrupted *rms* vertical beam size at IP vs. beam IP offset Δy (in undisrupted σ_y) in option H with E_{cms} = 490 GeV.

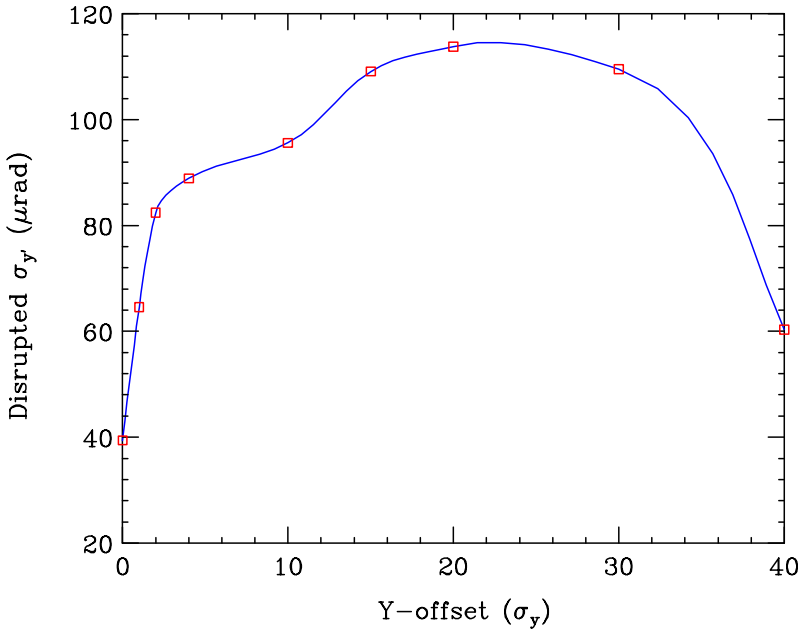

Figure 21: Disrupted *rms* vertical beam divergence at IP vs. beam IP offset Δy (in undisrupted σ_y) in option H with E_{cms} = 490 GeV.

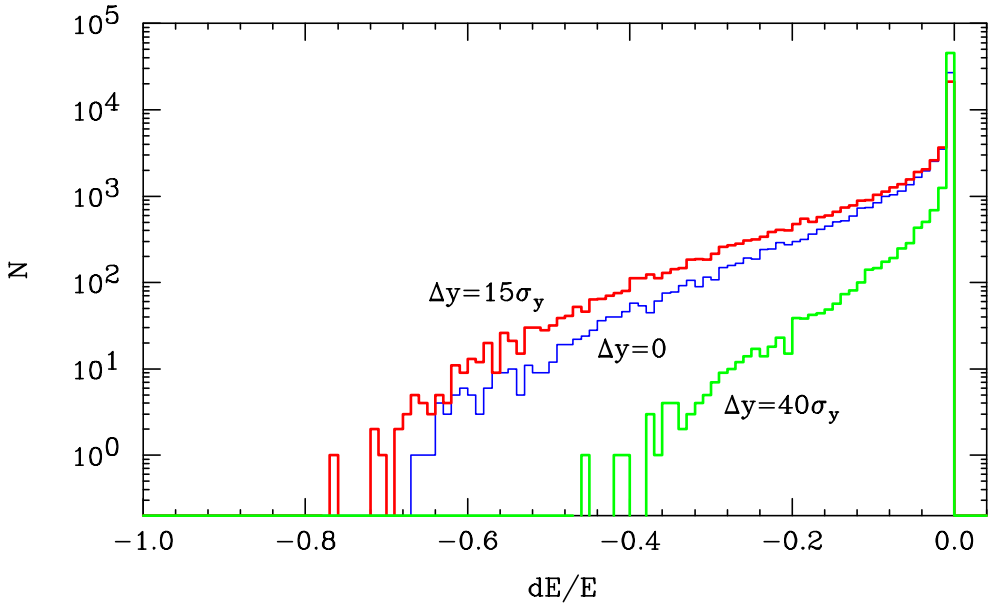

Figure 22: Disrupted energy distribution at IP with beam IP offset of $\Delta y = 0$, $15\sigma_y$ and $40\sigma_y$ in option H with $E_{cms} = 490$ GeV.

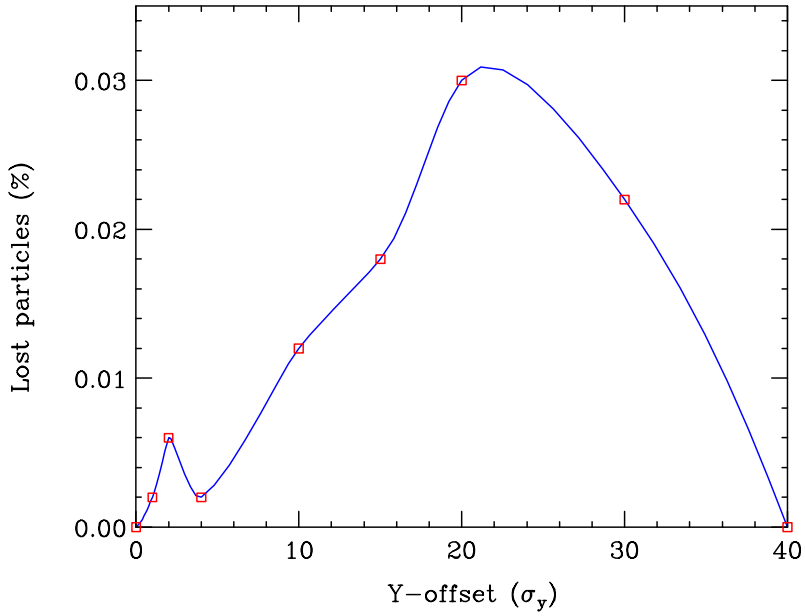

Figure 23: Particle loss in the extraction line vs. beam IP offset Δy (in undisrupted σ_y) in option H with $E_{cms} = 490$ GeV.

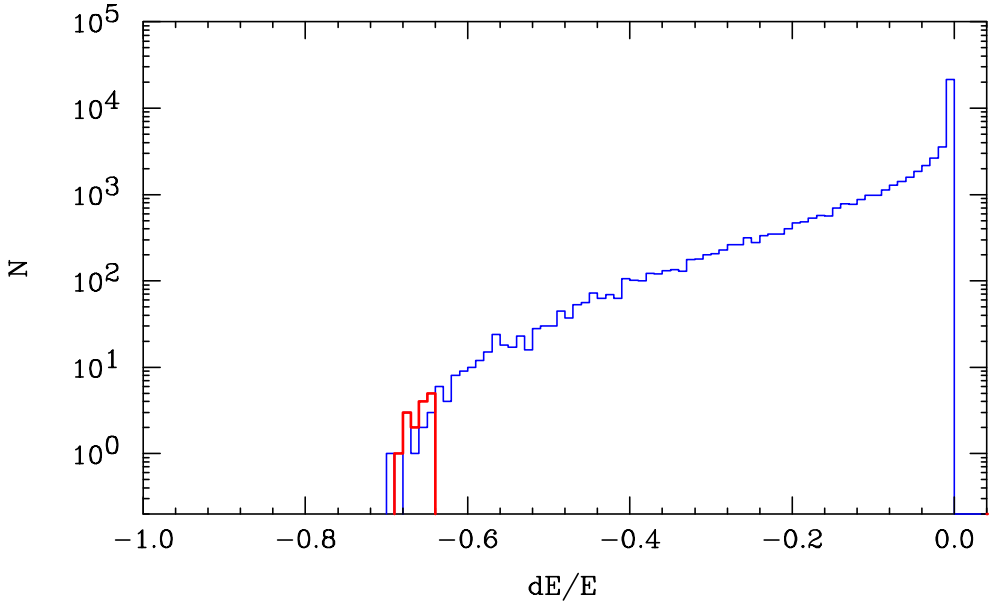

Figure 24: Disrupted energy distribution at IP for survived (thin line) and lost (thick) particles in option H with $E_{cms}=490$ GeV and beam IP offset $\Delta y=20\sigma_y$.

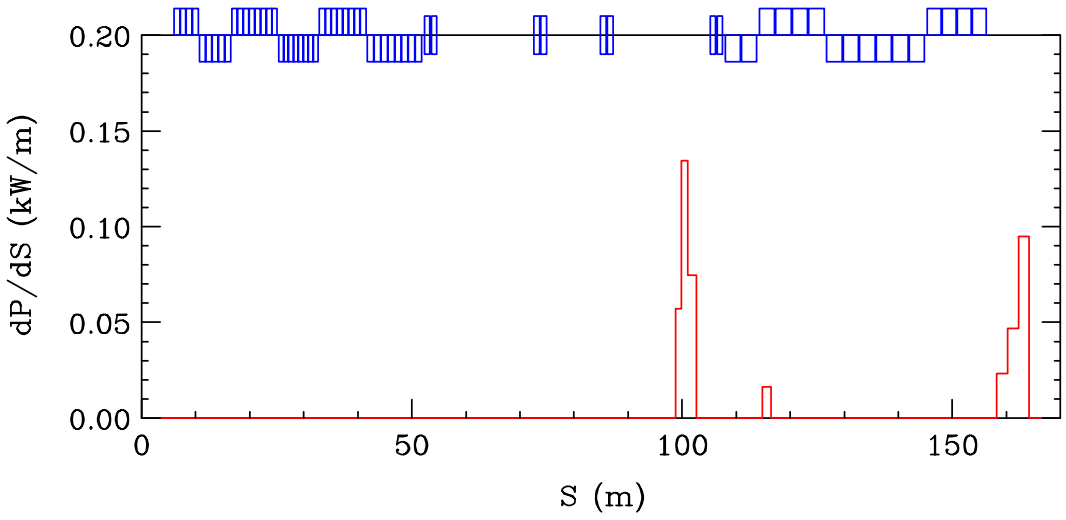

Figure 25: Beam power loss per meter $\frac{dP_{loss}}{ds}$ in the extraction line in option H with $E_{cms}=490$ GeV and beam IP offset $\Delta y=20\sigma_y$.

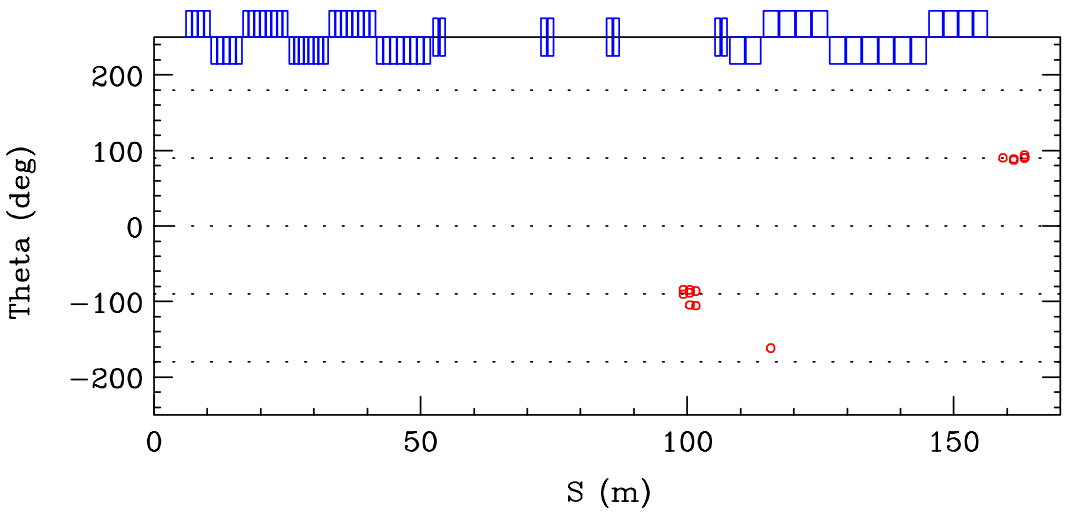

Figure 26: Azimuth positions of lost particles in the extraction line in option H with $E_{cms} = 490$ GeV and beam IP offset $\Delta y = 20\sigma_y$.